Journal of
Materials Chemistry A

PAPER

View Article Online
View Journal | View Issue

Cite this: *J. Mater. Chem. A*, 2019, 7, 10505

An extraordinary cyclohexylmethyl side chain dominating polymeric donor packing patterns and energy levels for efficient non-fullerene polymer solar cells†

Liangliang Han,[a] Nergui Uranbileg,[ab] Shengshi Jiang,[ab] Yu Xie,[a] Huanxiang Jiang,[ab] Zhenggang Lan,[a] Donghong Yu,*[cd] Xichang Bao*[a] and Renqiang Yang*[a]

Benefiting from the tremendous efforts devoted to small molecule electron acceptors (SMAs), great progress has been made in non-fullerene polymer solar cells (NF-PSCs). Yet compared with the structurally diverse SMAs, much less attention has been paid to polymeric donors, which are also extremely important components dominating the development of NF-PSCs. A material design concept for obtaining an easily achieved phase separated morphology between the polymeric donor and SMA is presented. The key concept lies in optimizing the polymer crystallinity, by inserting a newly developed cyclohexylmethyl side chain, thus improving the polymer:SMA miscibility, and simultaneously, decreasing the energy levels, and strengthening the overall packing of the polymers in their film states. Once the cyclohexylmethyl chains are introduced, PTAZ–*CH* and PTAZ–*CH*–S exhibit a higher absorption coefficient and deeper highest occupied molecular orbital (HOMO) energy levels, in comparison with the reference polymer. This methodology of using a cyclic side chain to control the polymer's crystallinity has the added benefits of forming optimal polymer:SMA morphologies without any post-treatments like thermal- or solvent-annealing, making such low energy consuming and environmentally friendly PSC fabrication available. Impressively, more than doubled power conversion efficiencies (PCEs) are obtained employing ordinary ITIC and IT-M as the electron accepting partners.

Received 4th March 2019
Accepted 23rd March 2019

DOI: 10.1039/c9ta02384d

rsc.li/materials-a

1. Introduction

Flexible, light-weight, solution-processable, and easily achieved low temperature large-area fabrication make polymer solar cells (PSCs) considered as a promising candidate for next generation photovoltaic (PV) technologies.[1–3] The design of new p-type donors[4,5] and n-type acceptors[6] as well as the optimization of the donor : acceptor bulk heterojunction (BHJ) structures[7,8] facilitate the rapid development of PSCs. In the past few decades, because of the lack of electron acceptors that can compete with fullerene derivatives, most advances in the device performance came from the design of new polymeric donors.[9–11] Therefore, a complementary low bandgap (LBG) polymer that has matching energy levels with fullerene acceptors is desirable. Recently, non-fullerene acceptors, particularly organic small molecule electron acceptors (SMAs),[12] whose energy levels and absorption can be reasonably regulated,[13–17] have emerged as a promising alternative to replace fullerene acceptors.[6] Consequently, a wide bandgap (WBG) polymer is more preferable to the LBG one in the 珐eld of non-fullerene PSCs (NF-PSCs).[18] Over the past three years, signi珐cant progress has been made in the 珐eld of NF-PSCs as a result of the extensive efforts devoted to the design of SMAs, which include (i) extending their optical absorption spectra towards a lower energy region that can create a large short-circuit current density (J_{SC});[19] (ii) enhancing their intermolecular interactions to improve the electron transport that is favored by a high 珐ll factor (FF);[20] and (iii) tailoring their lowest unoccupied molecular orbital (LUMO) energy levels to enlarge the open-circuit voltage (V_{OC}).[21] To date, over 13% and even 15% power conversion efficiency (PCE) has been reported for single-junction NF-PSCs based on different combinations of matured BDT structured polymeric donors and more creatively novel SMAs like IT-4F from Hou *et al.* (a derivative of ITIC) and Y6 from Zou *et al.* (A–DAD–A type with the core of

[a]*CAS Key Laboratory of Bio-based Materials, Qingdao Institute of Bioenergy and Bioprocess Technology, Chinese Academy of Sciences, Qingdao 266101, China. E-mail: baoxc@qibebt.ac.cn; yangrq@qibebt.ac.cn*

[b]*University of Chinese Academy of Sciences, Beijing, 100049, China*

[c]*Department of Chemistry and Bioscience, Aalborg University, DK-9220 Aalborg, Denmark. E-mail: yu@bio.aau.dk*

[d]*Sino-Danish Centre for Education and Research, Aarhus, DK-8000, Denmark*

† Electronic supplementary information (ESI) available: Device fabrication/testing, syntheses and characterization, DFT calculation, GPC measurement, UV-vis absorption coefficient, AFM, photoluminescence measurement, *J*–*V* curves, charge carrier mobility, GI-WAXS, NMR spectra, and HRMS spectra. See DOI: 10.1039/c9ta02384d

benzothiadiazole).[22,23] However, compared to SMAs, much less attention has been paid to polymeric donors. The matching of the polymeric donor with the SMA is crucial in achieving high PCE for NF-PSCs. Not only complementary absorption and appropriate energy levels are desired, but also, more importantly, a nano-scaled polymer:SMA interpenetrating network and well-de珋ned micro-structures are also of great importance. Although large varieties of WBG polymers have been reported and reviewed for PSCs, only a few of them are proven to match well with SMAs, such as WBG polymers containing benzo[1,2-*c*:4,5-*c*′]dithiophene-4,8-dione (BDD)[22,24–28] and 5,6-di珞uoro-2*H*-benzo[*d*][1,2,3]triazole (ffTAZ)[29,30] electron-withdrawing segments, which are strongly aggregated and highly crystalline, and have become the dominant donors for high performance NF-PSCs. Nevertheless, signi珋cantly, problems emerge as the polymer and SMA assemble during 珋lm casting from their mixed solution; in general, the polymer:SMA phase separation, micro-structures and domain size need to be optimized by means of post-treatments of either thermal- or solvent-annealing. In the case of the absence of such additional treatments, the PCEs of the NF-PSCs are relatively low, which reveals that the state-of-the-art polymer structure or con珋guration is not optimal enough to match with the SMA. An in-depth understanding of the polymer structures that govern the polymer:SMA morphology, and in turn, in珞uence the device performance becomes essential.

Unlike fullerene acceptors, SMAs have an anisotropic conjugated backbone, and the inter-molecular charge carrier transport in SMAs depends on the overlap of the p orbitals, and occurs mainly along the preferential p–p stacking direction. In addition, for SMAs, the bulky solubilizing side chains destroy the molecular arrangement, and result in structural disorder and weak crystallinity. Therefore, it is a great privilege to discover SMAs that adopt exceptional packing patterns and effectively transport electrons; fortunately, such a molecular geometry insight was provided by Jen *et al.*,[31] from the single crystal structure. It is just the structural characteristics, molecular packing, and the inter-molecular charge carrier transport mechanism of SMAs that should be responsible for their different donor selectivity compared to fullerene acceptors. Our previous work indicated that strongly aggregated polymers favored fullerene acceptors; in contrast, polymers with reduced aggregation matched better with SMAs.[32] However, the polymer structure–device property relationship is not very de珋nite; until now, there has been no straightforward basis guiding the design of polymers that can form an optimal phase-separated morphology with SMAs. Side chain engineering is a crucial aspect that can be utilized to control the polymer's aggregation, crystallinity and micro-structures in the blend 珋lms.[33] Particularly, a rational design may make the side chain a functional substituent to regulate the polymer's energy levels.[34] Here, a new cyclohexylmethyl (*CH*) chain is designed and gra泓ed onto ffTAZ and benzo[1,2-*b*:4,5-*b*′]dithiophene (BDT) alternating polymers, and two polymers with 2-ethylhexyl and 2-ethylhexylthio side chains on BDT units are constructed and named PTAZ–*CH* and PTAZ–*CH*–S, respectively, as depicted in Fig. 1a. *CH* chains are adopted in virtue of the distinctive

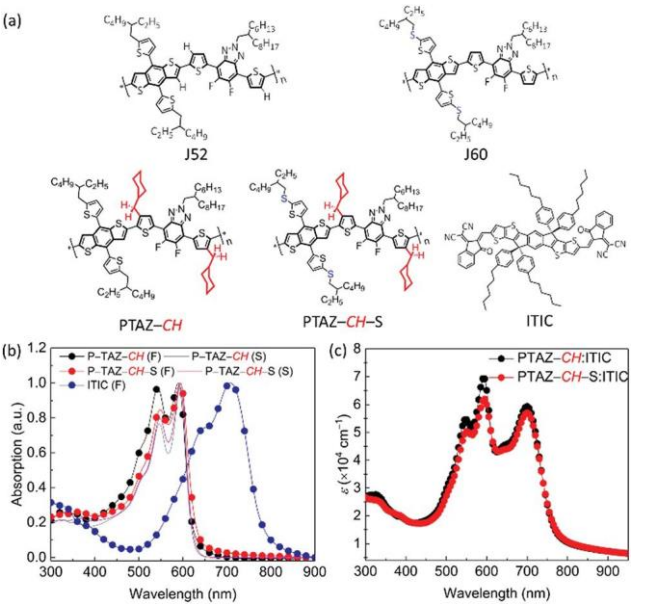

Fig. 1 Polymer structures (a), UV-vis absorption spectra of PTAZ–*CH*, PTAZ–*CH*–S and ITIC in solutions (S) and in films (F) (b), and polymer:ITIC blend films (c).

structural characteristics of cyclic chains, such as their rigidity and preferential "chair" conformations, which can promote the polymer self-assembly.[35] However, being different from our previous report, here a methylene group is inserted between the cyclohexyl and thiophene (TH) rings for the sake of the optimization of steric hindrance. Theoretical simulation (details in the Experimental section, ESI†) shows that once *CH* is introduced, the dihedral angle (q) between BDT and TH is enlarged from rv19.8° to rv38.0° (Fig. S1a†). Generally, a larger q will lead to a more tortuous backbone, and in turn, in珞uence the polymer aggregation and crystallinity. Further studies indicate that the *CH* chain is an extraordinary substituent that can make the backbone's overall packing more compact and decrease the polymer's highest occupied molecular orbital (HOMO) energy level, and besides, interestingly, PTAZ–*CH* and PTAZ–*CH*–S seem to have appropriate aggregation and exhibit excellent miscibility with SMAs, such as ITIC (9-bis(2-methylene-(3-(1,1-dicyanomethylene)-indanone))-5,5,11,11-tetrakis(4-hexylphenyl)-dithieno[2,3-*d*:2′,3′-*d*′]-*s*-indaceno[1,2-*b*:5,6-*b*′]dithiophene, Fig. 1a)[36] and IT-M (methyl-modi珋ed ITIC).[21] Finally, more than doubled PCEs are achieved compared to the reference polymer J52 (shown in Fig. 1a),[37] in the absence of any post-treatment for all the PTAZ–*CH*:ITIC, PTAZ–*CH*–S:ITIC, PTAZ–*CH*:IT-M and PTAZ–*CH*–S:IT-M PSCs, and the best PCE of 12.76% is obtained for the as-cast PTAZ–*CH*–S:IT-M device. The 珋lm structure characterization indicates that both of the polymers have highly crystalline micro-structures in their blend 珋lms, and continuous interpenetrating networks are established as well, ensuring high efficiency exciton separation, charge carrier transport and collection in the devices. The results indicate that there are large spaces to make polymers more compatible with SMAs, and ingeniously designed cyclic

alkyls are promising side chains for solution processed semiconducting polymers and as-cast devices.

2. Results and discussion

2.1. Synthesis

The synthetic routes of the polymers are provided in the Experimental section of the ESI and depicted in Scheme S1.† The monomer DBrTAZ-*CH* was synthesized using Stille coupling and then bromination in a proper sequence, and PTAZ-*CH* and PTAZ-*CH*-S were obtained through Pd(0) catalyzed Stille polymerization and purified using Soxhlet extraction. The number average molecular weight (M_n) of PTAZ-*CH* and PTAZ-*CH*-S is 68.61 kDa and 56.07 kDa with a corresponding polydispersity index (PDI) of 2.55 and 2.58, respectively, measured by gel permeation chromatography (GPC) using 1,2,4-trichlorobenzene as the eluent and carried out at 150 °C (Table 1 and Fig. S2†). They are readily dissolved in common solvents such as chloroform (CF), chlorobenzene (CB) and *o*-dichlorobenzene (*o*-DCB) at room temperature.

2.2. Photophysical and electrochemical properties

The UV-vis absorption spectra of PTAZ-*CH* and PTAZ-*CH*-S are shown in Fig. 1b and summarized in Table 1. In *o*-DCB solutions, the polymers have similar absorption profiles with two absorption peaks (λ_{max}) at 547 and 594 nm, respectively. Vibronic shoulder peaks can also be found in their film states, but obviously, PTAZ-*CH* has a relatively stronger shoulder λ_{max} at 542 nm compared to PTAZ-*CH*-S, which also differs from that of the reference J52. The discrepancy in the absorption profiles of the p-conjugated polymers that share the same backbone is closely interrelated with their aggregation or crystallinity in the solid films,[38,39] and a comparison will be presented and discussed in the Micro-structures section. Interestingly, PTAZ-*CH* and PTAZ-*CH*-S have a desirable absorption coefficient (ε) of ~9.75 × 10^4 and ~8.95 × 10^4 cm^{-1} in the film state (Fig. S3†), respectively, which are higher than that of J52 (3.7 × 10^4 cm^{-1}),[37] and a reasonable explanation will also be provided in the Micro-structures section. The optical bandgap (E_g^{opt}) of PTAZ-*CH* and PTAZ-*CH*-S is estimated to be ~2.00 and ~1.97 eV, being complementary to that of ITIC (1.59 eV),[36] and the polymer:ITIC blends cover a wide range of solar irradiation from 300–800 nm, combined with a high ε of ~6–7 × 10^4 cm^{-1} (Fig. 1c). A high ε and a wide optical absorption are favorable for large J_{SC}.[40,41]

As can be found from the electrochemical cyclic voltammetry (CV) data (Fig. 2, Table 1), PTAZ-*CH* has a high oxidation onset potential (E_{ox}) of ~0.89 V, and the E_{ox} of PTAZ-*CH*-S is further increased to ~0.93 V. Therefore, the HOMO energy levels (E_{HOMO}) of PTAZ-*CH* and PTAZ-*CH*-S are calculated to be −5.29 eV and −5.33 eV, respectively. The energy levels of the polymers and ITIC are depicted in Fig. 2b, and the LUMO energy levels (E_{LUMO}) of the polymers are calculated from their E_{HOMO} and E_g^{opt}, whereas the E_{HOMO} and E_{LUMO} of ITIC are calculated using a reported result.[36] Obviously, there is a respective down-shift of E_{HOMO} of about 0.08 eV and 0.12 eV for PTAZ-*CH* and PTAZ-*CH*-S compared to that of J52, and meanwhile, the E_{LUMO} also decreased. The deeper energy levels are probably ascribed to the reduction of p-electron delocalization as depicted in Fig. S1b,† which clearly shows more localized HOMO and LUMO distribution for PTAZ-*CH* compared to J52. The lower energy levels of the polymeric donors are likely to diminish the energy loss (E_{loss}) and favor higher V_{OC}.[42,43]

2.3. Micro-structures and morphologies of the polymers

The crystallinity and micro-structures of PTAZ-*CH* and PTAZ-*CH*-S are characterized using grazing incidence wide-angle X-ray scattering (GIWAXS, Fig. 3). As illustrated in Fig. 3a and b, pronounced (100) diffractions are observed in both the out-of-plane and in-plane directions, indicating that face-on and edge-on orientations coexist for both of the polymers. The lamellar packing distances (D_1) in the in-plane direction as revealed by (100) diffraction peaks (Fig. 3c and d) are ~19.94 Å and ~20.32 Å for PTAZ-*CH* and PTAZ-*CH*-S, respectively, while in the out-of-plane direction, it is ~14.67 Å for PTAZ-*CH* and ~15.46 Å for PTAZ-*CH*-S, indicating that the lamellar packing perpendicular to the substrate is more compact than that parallel to the substrate. By parallel comparison of these two polymers, it is found that the D_1 values are slightly enlarged when introducing sulfur atoms on the BDT unit, which agrees well with the

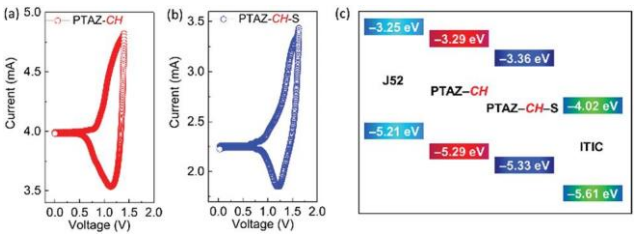

Fig. 2 CV curves of PTAZ-CH (a) and PTAZ-CH-S (b), and the energy level diagrams of PTAZ-CH, PTAZ-CH-S, ITIC, and the reference polymer J52 (c).

Table 1 Summary of the molecular weight and photophysical and electrochemical characteristics of PTAZ-*CH* and PTAZ-*CH*-S

Polymers	M_n [kDa]	M_w [kDa]	PDI [M_w/M_n]	ε [cm^{-1}]	λ_{edge} [nm]	E_g^{opt} [eV]	E_{HOMO} [eV]	E_{LUMO} [eV]
PTAZ-*CH*	68.61	174.95	2.55	9.75 × 10^4	619	2.00	−5.29	−3.29
PTAZ-*CH*-S	56.07	144.95	2.58	8.95 × 10^4	628	1.97	−5.33	−3.36

[a] Calculated from λ_{edge}: E_g^{opt} = 1240/λ_{edge}. [b] Calculated from electrochemical oxidation onset potential: E_{HOMO} = −e(E_{ox} + 4.40). [c] E_{LUMO} = E_g^{opt} + E_{HOMO}.

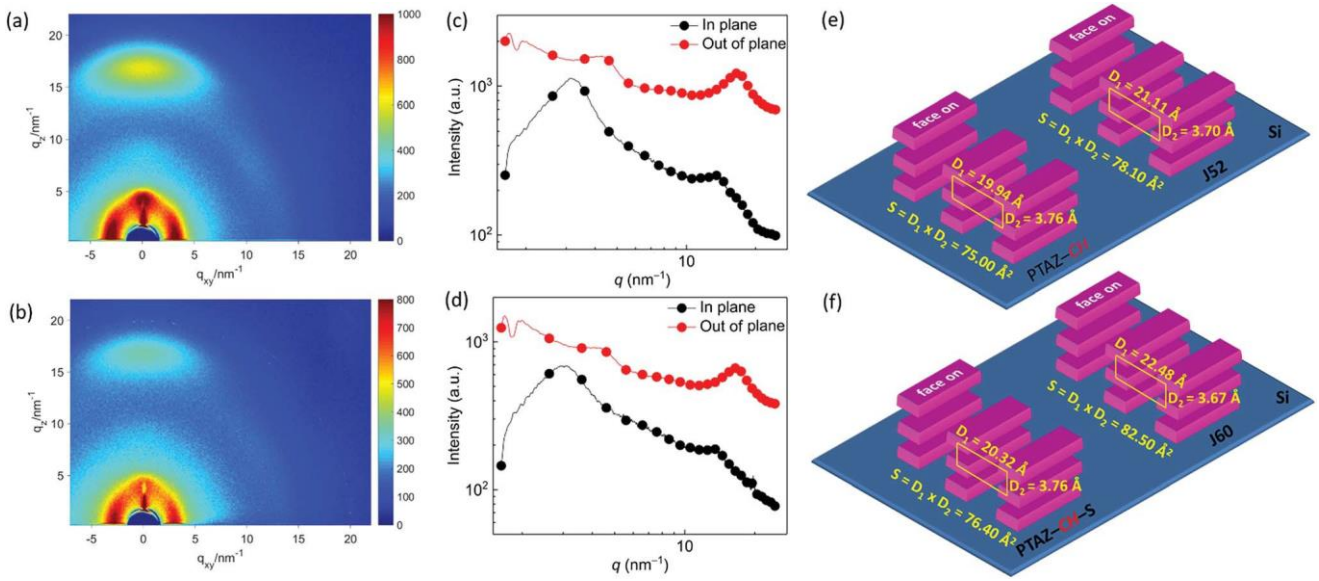

Fig. 3 2D-GIWAXS patterns (a, b), in-plane and out-of-plane GIWAXS profiles (c, d) of PTAZ-*CH* (top) and TAZ-*CH*-S (bottom) pristine films, and the stacking diagram of PTAZ-*CH* compared with that of J52 (e) and PTAZ-*CH*-S compared with that of J60 (see Fig. 1a) (f).

reported results because of the increased side chain length.[37] PTAZ-*CH* and PTAZ-*CH*-S also exhibit pronounced (010) diffractions in the out-of-plane direction with a nearly identical p-p stacking distance (D_2) of rv3.76 Å. The out-of-plane (010) and (100) and the in-plane (100) crystal coherence lengths (CCL) of PTAZ-*CH* are rv15.2 Å, 25.2 Å and 47.5 Å, respectively, while those for PTAZ-*CH*-S are rv10.8 Å, 23.8 Å and 40.1 Å, respectively. The larger CCL indicates higher crystallinity for PTAZ-*CH* than for PTAZ-*CH*-S, which could help to understand their different absorption pro珡les. A higher degree of crystallinity or packing order generally results in vibronic shoulder absorption. The crystalline micro-structures of PTAZ-*CH* and PTAZ-*CH*-S are also supported by the atomic force microscope (AFM) images as shown in Fig. S4,† which exhibit well-de珡ned networks on the surface of their pristine 珡lms.

The comparison of the packing patterns with and without the introduction of *CH* chains is also discussed. Fig. 3e and f show the stacking diagrams of the face-on orientated PTAZ-*CH* and PTAZ-*CH*-S together with those of the references J52 and J60 (found in Fig. 1a).[37] Obviously, PTAZ-*CH* and PTAZ-*CH*-S exhibit relatively looser p-p stacking characteristics with larger D_2 than that of J52 and J60, probably caused by the tortuous backbones. Instead, the lamellar packing of PTAZ-*CH* and PTAZ-*CH*-S tightened although it seems that extra *CH* may make the inter-chain interdigitation of the side chains more crowded, which may be due to their dislocation, and thus avoid direct docking and result in overall tighter lamellar packing. The D_1 decreased by about 1.17 Å for PTAZ-*CH* compared to that for J52 and 2.16 Å for PTAZ-*CH*-S compared to that for J60. In order to measure the overall compactness of the polymer packing, the product of D_1 and D_2 ($S = D_1 \times D_2$) is employed, and the *S* value is calculated to be about 75.00 Å^2 for PTAZ-*CH*, 76.40 Å^2 for PTAZ-*CH*-S, 78.10 Å^2 for J52 and 82.50 Å^2 for J60. The smaller *S* values of the newly designed polymers bene珡t from the decreased lamellar spacing, and indicate that the two additional *CH* chains on each BDT-ffTAZ repeating unit play crucial roles in promoting the polymer packing. On the other hand, a small *S* value also indicates high polymer backbone density in the 珡lm, which could help to explain the higher 3 of PTAZ-*CH* and PTAZ-*CH*-S compared to that of J52 and J60. The crystalline characteristics of a polymer with a loose p-p stacking but an overall tighter packing should be considered as one of the most critical factors that in珠uences its optical properties and will also affect its electrical and photovoltaic characteristics.

2.4. Photovoltaic properties

The photovoltaic performances of PTAZ-*CH* and PTAZ-*CH*-S are characterized using a conventional device con珡guration of ITO (indium tin oxide)/PEDOT:PSS (poly(3,4-ethylenedioxythiophene):polystyrene sulfonate)/polymer:ITIC/PFN-Br (poly[(9,9-bis(3′-((*N*,*N*-dimethyl)-*N*-ethylammonium)-propyl)-2,7-珠uorene)-*alt*-2,7-(9,9-dioctyl珠uorene)])/Al, and the detail fabrication is provided in the ESI.† ITIC is chosen as the electron acceptor due to its good complementary absorption to that of the ffTAZ-based polymers and matched E_{HOMO} and E_{LUMO}.[36] PFN-Br was adapted due to the fact that it is an efficient organic ETL material with less dependency on 珡lm thickness. The potential charge transfer occurring between the donor and acceptor is also estimated beforehand by measuring the photoluminescence (PL) of the neat PTAZ-*CH*, PTAZ-*CH*-S, and ITIC 珡lms and the polymer:ITIC blend 珡lms (Fig. S5†). PTAZ-*CH* and PTAZ-*CH*-S exhibit red emission (excited at 550 nm) with peak wavelengths centered at 663 and 641 nm, respectively, whose PL is quenched by ITIC at a high percent (rv98%). Meanwhile, the emission of ITIC (764 nm, excited at 700 nm) is also quenched by PTAZ-*CH* or PTAZ-*CH*-S at about 90%. The PL experiments suggest that most excitons (both in donors and

acceptors) are formed within the diffusion distance from the donor/acceptor interfaces, and subsequently, the photo-generated excitons diffuse substantially to the polymer/ITIC interfaces, where excitons are dissociated and charge carriers are generated, and then charge transfer occurs.[44] Generally, the mutual 珍uorescence quenching between the donor and acceptor re珍ects a good donor : acceptor miscibility besides their well-matched energy levels.

The optimized polymer concentration for PTAZ-*CH* and PTAZ-*CH*-S is 7.5 and 10 mg mL^{-1} in CB solution, respectively, with a polymer:ITIC ratio of 1 : 1 wt%. The best device performance (Table 2) is obtained at a spin rate of 1800 rpm (rv110 nm) for PTAZ-*CH*:ITIC and 2500 rpm (rv114 nm) for PTAZ-*CH*-S:ITIC, and the optimization of the spinning is summarized in Table S1.† Fig. 4a shows the current density–voltage (*J*-*V*) together with the power output curves of the optimized PTAZ-*CH*:ITIC and PTAZ-*CH*-S:ITIC based devices (100 mW cm^{-2} (AM 1.5G) irradiation). In comparison with the reference J52:ITIC blend, for which the as-cast PSC exhibited a low PCE of 5.18% with E_{loss}(E_g — eV_{OC}) as high as 0.83–0.84 eV, and even a沢er a thermal annealing (TA) optimization, the PCE was still below 6%.[37] A沢er introducing *CH* chains, the E_{loss} is sharply decreased to 0.71 eV, and the PCE of the PTAZ-*CH*:ITIC based device has been more than doubled, up to 11.28%, with a signi珍cantly improved V_{OC} of 0.89 V, J_{SC} of 18.20 mA cm^{-2} and FF of 70.04%. The higher V_{OC} of PTAZ-*CH*:ITIC is mainly ascribed to the deeper E_{HOMO} of PTAZ-*CH*. The improvement of J_{SC} is partially because of the higher 3 of PTAZ-*CH* than J52 as described above, and also is related to the effective exciton dissociation and suppressed charge recombination in the device, which will be discussed in the following section. For PTAZ-*CH*-S:ITIC, the use of alkylthio as well as *CH* chains increases the V_{OC} up to 0.94 V, and the E_{loss} is strongly restrained and reduced to 0.65 eV. Although the J_{SC} (17.61 mA cm^{-2}) decreases slightly compared to that of PTAZ-*CH*:ITIC (relatively lower 3 of PTAZ-*CH*-S:ITIC BHJ illustrated in Fig. 1c), the FF increases to 73.18%, and as a result, the overall PCE of the PTAZ-*CH*-S:ITIC based device reaches up to 12.15%. This value is obtained for the as-cast active layer without any additive and post-treatment, which has been rarely reported for non-fullerene PSCs,[45] particularly for ffTAZ-based polymers. The devices treated by TA are also investigated, and the *J*-*V* curves are shown in Fig. S6† and the device parameters are summarized in Table S2.† However, the PCE decreased slightly, indicating that TA is not the necessary process for PTAZ-*CH*:ITIC and PTAZ-*CH*-S:ITIC based PSCs, which also implies an optimal polymer:ITIC phase separation morphology for the as-cast 珡lms. PTAZ-*CH*:ITIC and PTAZ-*CH*-S:ITIC exhibit a broad photo-response from 300–800 nm, which can be observed from the external quantum efficiency (EQE) spectra as illustrated in Fig. 4b, with maximal EQE approaching 80%. The J_{SC} integrated from the EQE spectra is in good agreement with that obtained from *J*-*V* measurements (Fig. 4b).

The series resistance (R_s) and the shunt resistance (R_{sh}) determine where the current 珍ows, and are one of the most important factors that limit the parameters of a PSC.[46] As summarized in Table 2, the PTAZ-*CH*:ITIC and PTAZ-*CH*-S:ITIC based cells have a small R_s (the inverse slope at $V \approx V_{OC}$ in *J*-*V* curves under illumination) of 5.25 Ω cm^2 and 4.56 Ω cm^2, respectively, indicating that the current will mainly 珍ow into the diodes and show a trend of rapid growth as the voltage increases. Meanwhile, the two devices have a large R_{sh} (the inverse slope at $V \approx 0$ in *J*-*V* curves under illumination) of 1573.98 Ω cm^2 and 1282.41 Ω cm^2, respectively, which will decrease the current loss at the interfaces or in the active layers. Therefore, the low R_s and large R_{sh} in the PTAZ-*CH*:ITIC and PTAZ-*CH*-S:ITIC based devices will help understand the observation of high FF and J_{SC}.[47] In view of the conventional device structure employed in this work (the electrodes, functional layers, and their interfaces are similar compared to other PSCs with such a device structure), the high device performance especially the FF will mainly be ascribed to high-quality ploymer:ITIC 珡lms, which indicates that the as-cast PTAZ-*CH*:ITIC and PTAZ-*CH*-S:ITIC 珡lms have satisfactory morphologies. The dark *J*-*V* curves are also presented to estimate the diode characteristics of the related devices as shown in Fig. 4c. The shape of the dark *J*-*V* curves reveals typical diode characteristics for both devices, and the diodes show a low dark saturation current density (J_0) of rv1.31×10^{-9} and rv7.19×10^{-10} mA cm^{-2} (by exponential 珡tting of the dark *J*-*V* curves), respectively.[48] Subsequently, the ideality factor (n) can be calculated from the simpli珡ed Shockley equation according to the literature:

$$J \approx J_0 \exp\left(\frac{qV}{nk_BT}\right) - 1$$

where *J* is the injected current density, *V* is the applied voltage, q is the elementary charge, k_B is the Boltzmann constant, and *T* is the temperature.[48] For PTAZ-*CH*:ITIC, $n \approx 1.60$, and for PTAZ-*CH*-S:ITIC, $n \approx 1.62$, and the relatively small n values together with low J_0 illustrate the good diode characteristics of the PTAZ-*CH*:ITIC and PTAZ-*CH*-S:ITIC based devices.

Table 2 Summary of the device parameters for PTAZ-*CH*:ITIC and PTAZ-*CH*-S:ITIC based PSCs

Blends	V_{OC}[c] (V)	J_{SC}[c] (mA cm^{-2})	FF[c] (%)	PCE[c] (%)	R_s (Ω cm^2)	R_{sh} (Ω cm^2)	m_h (cm^2 V^{-1} s^{-1})	m_e (cm^2 V^{-1} s^{-1})
A[a]	0.89 (0.89 ± 0.01)	18.20 (17.98 ± 0.31)	70.04 (69.96 ± 0.97)	11.35 (11.18 ± 0.05)	5.25	1573.98	5.31×10^{-4}	0.94×10^{-4}
B[b]	0.94 (0.95 ± 0.04)	17.61 (17.36 ± 0.17)	73.18 (72.26 ± 0.59)	12.15 (11.86 ± 0.17)	4.56	1282.41	6.30×10^{-4}	0.80×10^{-4}

[a] As-cast PTAZ-*CH*:ITIC. [b] As-cast PTAZ-*CH*-S:ITIC. [c] The standard deviations of the device parameters are obtained from 8 devices.

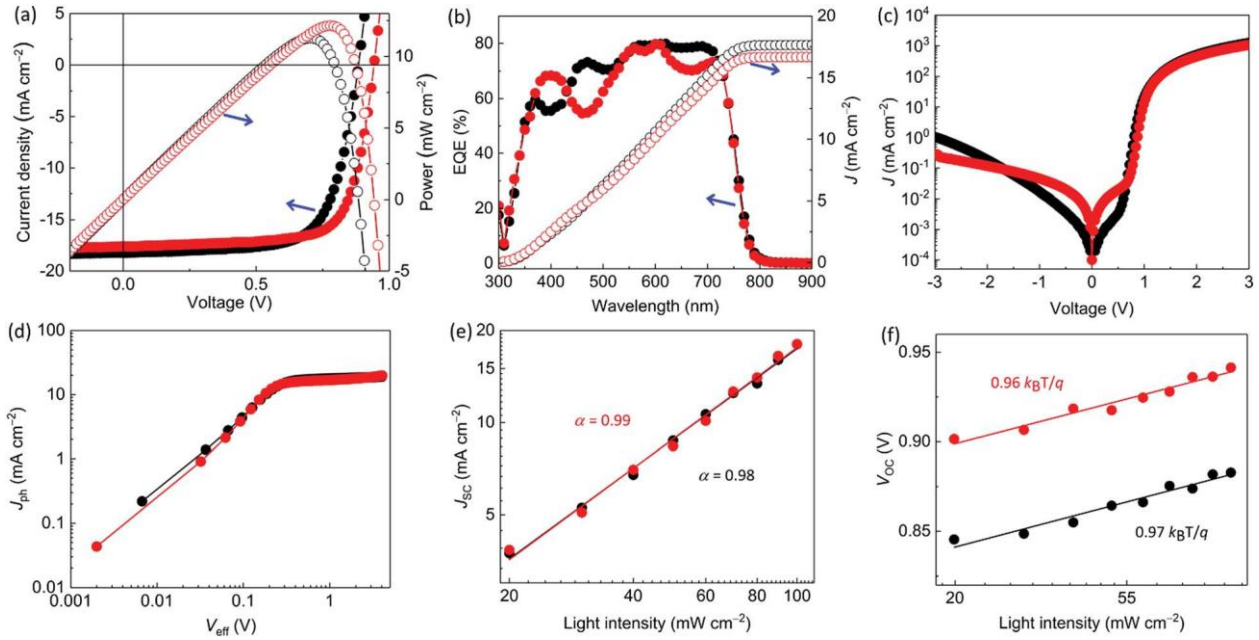

Fig. 4 *J*–*V* and power output curves (a), EQE and the integrated *J* curves (b), dark *J*–*V* curves (c), J_{ph}–V_{eff} curves (d), J_{SC}–P_{light} curves (e), and V_{OC}–P_{light} curves (f) of PTAZ-*CH*:ITIC (black) and PTAZ-*CH*-S:ITIC (red) based PSCs.

2.5. Exciton dissociation and charge recombination

The plots of photocurrent density (J_{ph}) *versus* effective applied voltage (V_{eff}) are depicted in Fig. 4d, to characterize the exciton dissociation and charge collection of the devices.[49] The effective experimental photocurrent density is given by $J_{ph} = J_L - J_D$, where J_L and J_D are the photocurrent densities under illumination and in the dark, respectively. V_{eff} is given by $V_{eff} = V_0 - V_{appl}$, where V_0 is defined as the voltage where $J_L = J_D$ and V_{appl} is the applied bias.[50] J_{ph} is plotted on a double logarithmic scale against V_{eff}. For the PTAZ-*CH*:ITIC device, J_{ph} is saturated at V_{eff} > 1.7 V, and the saturated photocurrent density (J_{sat}) is 18.9 mA cm^{-2}; therefore, the charge extraction probability (J_{ph}/J_{sat}) is estimated to be as high as 96% under short-circuit conditions, and 86% under the maximal power output (J_{ph} = 16.28 mA cm^{-2}) conditions. For the PTAZ-*CH*-S:ITIC device, J_{ph} is saturated at V_{eff} > 1.8 V, and J_{sat} is 18.2 mA cm^{-2}, resulting in a J_{ph}/J_{sat} of 97% and 86%, respectively, under the short-circuit and maximal power output (J_{ph} = 15.57 mA cm^{-2}) conditions. The high charge extraction probabilities indicate sufficient exciton dissociation and effective charge collection in both devices.[51] The J_{ph} saturated at large bias suggests that the mean electron and hole drift lengths are equal to or larger than the device thickness and no recombination occurs.

To gain deeper insight into the charge recombination, we investigate the variation of J_{SC} as a function of light intensity (P_{light}) using the power-law equation $J_{SC} \propto P_{light}^{\alpha}$; if the power-law exponent α is close to 1, it is taken as indicative of weak bimolecular recombination.[52] The log–log plots of J_{SC} *versus* P_{light} are shown in Fig. 4e, and thus, the α values are deduced as the slope of the linear fitting curves, being 0.98 and 0.99, respectively, for PTAZ-*CH*:ITIC and PTAZ-*CH*-S:ITIC devices, indicating negligible bimolecular recombination. The P_{light} dependent V_{OC} variations ($V_{OC} \propto \ln P_{light}$) are also studied to investigate the charge recombination behaviors besides the bimolecular recombination. The plots of V_{OC} *versus* P_{light} are shown in Fig. 4f, where the abscissa is defined as the natural logarithm of P_{light}, and the slope of the linear fitting curves of PTAZ-*CH*:ITIC and PTAZ-*CH*-S:ITIC devices is 0.97 and 0.96 k_BT/q, respectively, which are very close to k_BT/q, implying that the Shockley–Read–Hall or trap-assisted recombination is incredibly low. These physical experiments provide strong evidence for high exciton dissociation probability and charge collection efficiency as well as effective charge recombination supersession in our solar cells, which can substantially explain the high J_{SC} and FF of the devices.

The charge carrier mobility of the devices is measured using the space-charge-limited current (SCLC) method (details are provided in the Experimental section of the ESI†). The *J*–*V* curves of the hole only and electron only devices are shown in Fig. S7.† The hole mobility (μ_h) of PTAZ-*CH*:ITIC and PTAZ-*CH*-S:ITIC is calculated to be 5.81×10^{-4} and 6.30×10^{-4} cm^2 V^{-1} s^{-1}, respectively, higher than that of most of the polymers used for NF-PSCs in their as-cast films or even with post-treatments.[37] The electron mobility (μ_e) of the as-cast PTAZ-*CH*:ITIC and PTAZ-*CH*-S:ITIC films is 0.94×10^{-4} and 0.80×10^{-4} cm^2 V^{-1} s^{-1}, respectively, being relatively lower than the μ_h of the film, but comparable to the literature reports.[36,53] It should be noted that although ITIC is a widely used SMA, it has weak crystallinity and relatively low μ_e in the as-cast film, which limits its application for the as-cast PSCs. Therefore, the high device performances in this work are certainly ascribed to the successful design strategy of the polymer donors, and better device parameters are expected when using other SMAs with high crystallinity and μ_e.

2.6. Micro-structures and morphologies of the polymer:ITIC blends

The 2D-GIWAXS and line cut profiles of the PTAZ-*CH*:ITIC and PTAZ-*CH*-S:ITIC films are shown in Fig. 5. Both the as-cast blend films exhibit strong crystalline diffractions. However, ITIC seems less crystalline, which is further confirmed by its 2D-GIWAXS pattern for the pristine film (Fig. S8†). The weak crystallinity of ITIC is in agreement with Wei's report,[54] implying the disordered packing of ITIC, which is likely to explain the low m_e of the blend films. The polymers exhibit similar crystalline characteristics to their pristine films, with a strong out-of-plane (010) diffraction together with (100) diffractions in both the in-plane and out-of-plane directions. The D_2 value calculated from Fig. 5c and d is ~3.62 Å and ~3.67 Å, respectively, for PTAZ-*CH* and PTAZ-*CH*-S, diminished compared with ~3.76 Å in their pristine films. The D_1 values in the out-of-plane (18.43 Å for PTAZ-*CH* and 19.10 Å for PTAZ-*CH*-S) and in-plane (14.47 Å for PTAZ-*CH* and 14.94 Å for PTAZ-*CH*-S) directions are also smaller than those in the pristine films, indicating more compact packing for the polymers in the blend films (the *S* value is 66.72 Å^2 for PTAZ-*CH* and 70.10 Å^2 for PTAZ-*CH*-S). We infer that the overall tighter packing in the blends than in the pristine films for the polymers originated from the polymer chain re-organization. Supposing that a polymer has too strong aggregation characteristics (tight p-p stacking), the polymer chains will pre-aggregate together even in the solution phase,[55] and subsequently, exhibit poor self-assembly behavior. The pre-aggregated polymers, apparently, will show identical stacking characteristics with similar D_1 and D_2 values. However, when a polymer has moderate aggregation (loose p-p stacking), such as PTAZ-*CH* or PTAZ-*CH*-S, it will disperse in the solution with a certain non-aggregated state. Therefore, self-assembly occurs during spin coating, which is very important for the observation of highly ordered micro-structures in the film. The tighter packing patterns of PTAZ-*CH* and PTAZ-*CH*-S in their blend films are probably correlated with the different composition when ITIC is also dissolved in CB. The CCL of (010) diffraction is 7.49 Å for PTAZ-*CH*, while it is 7.99 Å for PTAZ-*CH*-S, indicating slightly stronger crystallinity of PTAZ-*CH*-S, which reverses compared to the pristine polymer films. The higher degree of packing order results in slightly higher m_h of PTAZ-*CH*-S in the blend film despite the relatively larger D_2 value.

The surface and inner micro-structures of polymer:ITIC blend films are also investigated using an AFM and transmission electron microscope (TEM), respectively, which are shown in Fig. 6. PTAZ-*CH*:ITIC and PTAZ-*CH*-S:ITIC exhibit a desirable film-forming ability with smooth and uniform surface morphologies, which are accompanied by well-defined structures as well as small root-mean-square (RMS) surface roughness of 1.39 nm and 1.15 nm, respectively, as seen from their AFM height images (Fig. 6a and b). Moreover, continuous interpenetrating micro-structures for both the BHJ films are observed from their TEM images (Fig. 6c and d) without severe phase separation and large polymers or ITIC domains. The microscopy together with the GIWAXS analyses support strongly the observation of good miscibility between the donor and acceptor, which is favorable for high exciton dissociation and charge carrier transport and collection.

In order to further verify the feasibility of the material design concept, another widely accepted molecule IT-M is also chosen as the acceptor.[21] The *J*–*V* curves and device parameters are provided in the ESI (Fig. S9 and Table S3†). Interestingly, PTAZ-*CH* and PTAZ-*CH*-S also match well with IT-M, and even higher PCEs of 12.22% and 12.76% are obtained combined with high FFs of over 70% under various preparation conditions, which implies good morphologies for the as-cast polymer:IT-M films. These results convincingly suggest that such a design strategy of polymeric donors is promising for NF-PSCs.

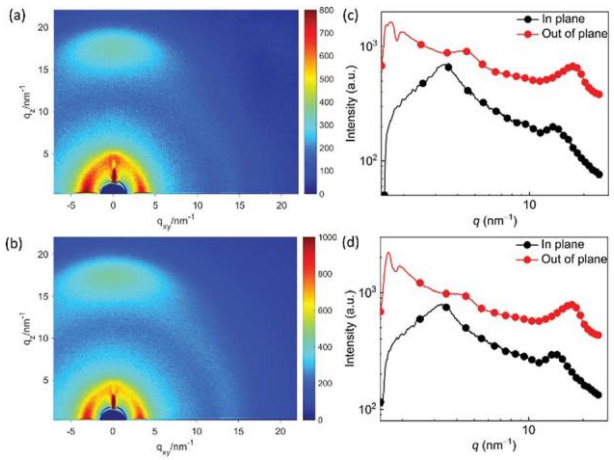

Fig. 5 2D-GIWAXS patterns (a, b) and in-plane and out-of-plane GIWAXS profiles (c, d) of PTAZ-*CH*:ITIC (top) and PTAZ-*CH*-S:ITIC (bottom) blend films.

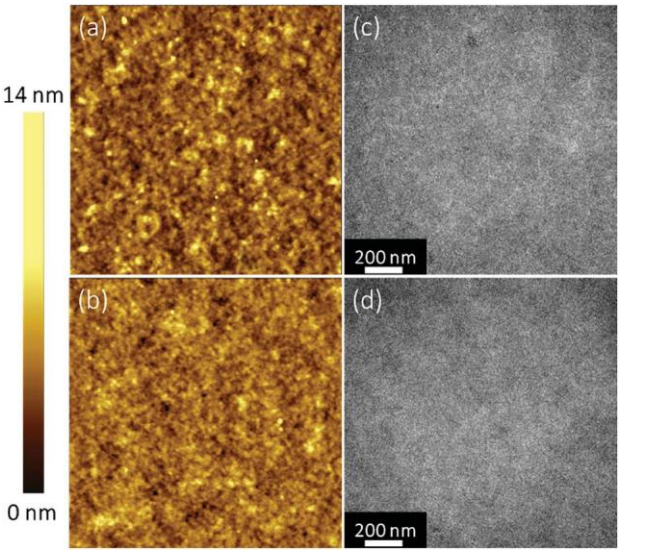

Fig. 6 AFM height (5 × 5 mm (a, b)) and TEM (c, d) images of PTAZ-*CH*:ITIC (top) and PTAZ-*CH*-S:ITIC (bottom) blend films.

3. Conclusions

In summary, our studies provide a new insight to design polymeric donors for NF-PSCs. We demonstrate that, 珋rstly, more twisted polymer backbones, prepared by inserting bulky alkyl chains, indeed bene珋t obtaining a polymer:SMA phase separation morphology, even though they are considered not favorable for inter-molecular stacking. Secondly, the tortuous polymer backbones reduce the p-electron delocalization, and thus decrease the frontier molecular orbit energy levels. Thirdly, the gra泓ing cyclohexylmethyl chain strengthens the side chain interdigitation, and results in overall tighter packing patterns, which endow PTAZ-*CH* and PTAZ-*CH*-S with high 3. These characteristics provide great bene珋t for solar cells. Continuously PTAZ-*CH*:ITIC and PTAZ-*CH*-S:ITIC exhibit high efficiency up to 11.28% and 12.15%, respectively, being much higher than that of reference J52:ITIC based solar cells, for which a moderate PCE of 5.18% was reported. In virtue of the decent miscibility between the donor and acceptor, the as-cast PTAZ-*CH*:ITIC and PTAZ-*CH*-S:ITIC 珋lms show optimal morphologies and phase separation structures, which enable highly efficient exciton dissociation, charge carrier transport and collection, and signi珋cantly suppressed charge recombination in the devices as well. It is worth noting that PTAZ-*CH* and PTAZ-*CH*-S are also adapt- able for IT-M, and the PTAZ-*CH*:IT-M and PTAZ-*CH*-S:IT-M based PSCs exhibit an even higher PCE of 12.22% and 12.76%, respectively, in the absence of any post-treatment, which are among the highest values reported so far for the easily fabricated NF-PSCs. Our work exhibits a material design concept with high signi珋cance for the environmentally friendly achievement of high performance NF-PSCs, with low energy consumption in the absence of either thermal- or solvent-annealing.

Conflicts of interest

The authors have no con珍icts to declare.

Acknowledgements

This work was supported by the National Natural Science Foundation of China (51873227, 51503219, 51573205 and 51773220), the Shandong Provincial Natural Science Foundation (ZR2015EQ002 and ZR2017ZB0314), the Qingdao Applied and Fundamental Research (16-5-1-94-jch), DICP & QIBEBT (UN201709), and the Dalian National Laboratory for Clean Energy (DNL), CAS. X. Bao thanks the Youth Innovation Promotion Association CAS (2016194) for 珋nancial support. The authors thank Dr Chunming Yang and the beamline BL16B1 (Shanghai Synchrotron Radiation Facility) for the GIWAXS test. D. Yu thanks Innovation Fund Denmark (INKA-Inks for large-scale processing of polymer solar cells). Support from the Sino-Danish Center for Education and Research (SDC) is fully acknowledged.

Notes and references

1 G. Yu, J. Gao, J. C. Hummelen, F. Wudl and A. J. Heeger, *Science*, 1995, 270, 1789–1791.
2 A. C. Arias, J. D. MacKenzie, I. McCulloch, J. Rivnay and A. Salleo, *Chem. Rev.*, 2010, 110, 3–24.
3 G. Li, R. Zhu and Y. Yang, *Nat. Photonics*, 2012, 6, 153–161.
4 J. B. Zhao, Y. K. Li, G. F. Yang, K. Jiang, H. R. Lin, H. Ade, W. Ma and H. Yan, *Nat. Energy*, 2016, 1, 7.
5 J. Yaocheng, C. Zhiming, X. Manjun, P. Jiajun, F. Baobing, Y. Lei, Z. Guichuan, J. Xiao-Fang, Y. Qingwu, L. Ziqi, H. Fei and C. Yong, *Adv. Energy Mater.*, 2017, 7, 1700944.
6 G. Zhang, J. Zhao, P. C. Y. Chow, K. Jiang, J. Zhang, Z. Zhu, J. Zhang, F. Huang and H. Yan, *Chem. Rev.*, 2018, 118, 3447–3507.
7 J. K. Lee, W. L. Ma, C. J. Brabec, J. Yuen, J. S. Moon, J. Y. Kim, K. Lee, G. C. Bazan and A. J. Heeger, *J. Am. Chem. Soc.*, 2008, 130, 3619–3623.
8 G. Li, V. Shrotriya, J. Huang, Y. Yao, T. Moriarty, K. Emery and Y. Yang, *Nat. Mater.*, 2005, 4, 864.
9 L. Lu, T. Zheng, Q. Wu, A. M. Schneider, D. Zhao and L. Yu, *Chem. Rev.*, 2015, 115, 12666–12731.
10 J. Li, Z. Liang, Y. Wang, H. Li, J. Tong, X. Bao and Y. Xia, *J. Mater. Chem. C*, 2018, 6, 11015–11022.
11 J. Li, Y. Wang, Z. Liang, N. Wang, J. Tong, C. Yang, X. Bao and Y. Xia, *ACS Appl. Mater. Interfaces*, 2019, 11, 7022–7029.
12 Y. Lin and X. Zhan, *Acc. Chem. Res.*, 2016, 49, 175–183.
13 S. Holliday, R. S. Ashraf, A. Wadsworth, D. Baran, S. A. Yousaf, C. B. Nielsen, C. H. Tan, S. D. Dimitrov, Z. Shang, N. Gasparini, M. Alamoudi, F. Laquai, C. J. Brabec, A. Salleo, J. R. Durrant and I. McCulloch, *Nat. Commun.*, 2016, 7, 11585.
14 Y. Lin, F. Zhao, Q. He, L. Huo, Y. Wu, T. C. Parker, W. Ma, Y. Sun, C. Wang, D. Zhu, A. J. Heeger, S. R. Marder and X. Zhan, *J. Am. Chem. Soc.*, 2016, 138, 4955–4961.
15 H. Yao, Y. Cui, R. Yu, B. Gao, H. Zhang and J. Hou, *Angew. Chem., Int. Ed.*, 2017, 56, 3045–3049.
16 Y. Li, J.-D. Lin, X. Che, Y. Qu, F. Liu, L.-S. Liao and S. R. Forrest, *J. Am. Chem. Soc.*, 2017, 139, 17114–17119.
17 S. Chen, H. Yao, Z. Li, O. M. Awartani, Y. Liu, Z. Wang, G. Yang, J. Zhang, H. Ade and H. Yan, *Adv. Energy Mater.*, 2017, 7, 1602304.
18 Y. Cai, L. Huo and Y. Sun, *Adv. Mater.*, 2017, 29, 1605437.
19 Y. Li, L. Zhong, B. Gautam, H.-J. Bin, J.-D. Lin, F.-P. Wu, Z. Zhang, Z.-Q. Jiang, Z.-G. Zhang, K. Gundogdu, Y. Li and L.-S. Liao, *Energy Environ. Sci.*, 2017, 10, 1610–1620.
20 S. Li, L. Ye, W. Zhao, X. Liu, J. Zhu, H. Ade and J. Hou, *Adv. Mater.*, 2017, 29, 1704051.
21 S. Li, L. Ye, W. Zhao, S. Zhang, S. Mukherjee, H. Ade and J. Hou, *Adv. Mater.*, 2016, 28, 9423–9429.
22 W. Zhao, S. Li, H. Yao, S. Zhang, Y. Zhang, B. Yang and J. Hou, *J. Am. Chem. Soc.*, 2017, 139, 7148–7151.
23 J. Yuan, Y. Zhang, L. Zhou, G. Zhang, H.-L. Yip, T.-K. Lau, X. Lu, C. Zhu, H. Peng, P. A. Johnson, M. Leclerc, Y. Cao, J. Ulanski, Y. Li and Y. Zou, *Joule*, 2019, 3, 1–12.

24 H. Zhang, H. Yao, J. Hou, J. Zhu, J. Zhang, W. Li, R. Yu, B. Gao, S. Zhang and J. Hou, *Adv. Mater.*, 2018, 30, 1800613.
25 T. Liu, L. Huo, S. Chandrabose, K. Chen, G. Han, F. Qi, X. Meng, D. Xie, W. Ma, Y. Yi, J. M. Hodgkiss, F. Liu, J. Wang, C. Yang and Y. Sun, *Adv. Mater.*, 2018, 30, 1707353.
26 T. Liu, X. Pan, X. Meng, Y. Liu, D. Wei, W. Ma, L. Huo, X. Sun, T. H. Lee, M. Huang, H. Choi, J. Y. Kim, W. C. H. Choy and Y. Sun, *Adv. Mater.*, 2017, 29, 1604251.
27 H. Fu, Z. Wang and Y. Sun, *Angew. Chem., Int. Ed.*, 2019, 58, 4442–4453.
28 L. Ye, Y. Xie, K. Weng, H. S. Ryu, C. Li, Y. Cai, H. Fu, D. Wei, H. Y. Woo, S. Tan and Y. Sun, *Nano Energy*, 2019, 58, 220–226.
29 Y. Lin, F. Zhao, S. K. K. Prasad, J.-D. Chen, W. Cai, Q. Zhang, K. Chen, Y. Wu, W. Ma, F. Gao, J.-X. Tang, C. Wang, W. You, J. M. Hodgkiss and X. Zhan, *Adv. Mater.*, 2018, 30, 1706363.
30 H. Bin, L. Gao, Z.-G. Zhang, Y. Yang, Y. Zhang, C. Zhang, S. Chen, L. Xue, C. Yang, M. Xiao and Y. Li, *Nat. Commun.*, 2016, 7, 13651.
31 X. Shi, L. Zuo, S. B. Jo, K. Gao, F. Lin, F. Liu and A. K. Y. Jen, *Chem. Mater.*, 2017, 29, 8369–8376.
32 D. Liu, J. Wang, C. Gu, Y. Li, X. Bao and R. Yang, *Adv. Mater.*, 2018, 30, 1705870.
33 J. Mei and Z. Bao, *Chem. Mater.*, 2014, 26, 604–615.
34 L. Han, W. Chen, T. Hu, J. Ren, M. Qiu, Y. Zhou, D. Zhu, N. Wang, M. Sun and R. Yang, *ACS Macro Lett.*, 2015, 4, 361–366.
35 L. Han, H. Jiang, D. Ouyang, W. Chen, T. Hu, J. Wang, S. Wen, M. Sun and R. Yang, *Nano Energy*, 2017, 36, 110–117.
36 Y. Lin, J. Wang, Z. G. Zhang, H. Bai, Y. Li, D. Zhu and X. Zhan, *Adv. Mater.*, 2015, 27, 1170–1174.
37 H. Bin, Z.-G. Zhang, L. Gao, S. Chen, L. Zhong, L. Xue, C. Yang and Y. Li, *J. Am. Chem. Soc.*, 2016, 138, 4657–4664.
38 X. Guo, N. Zhou, S. J. Lou, J. W. Hennek, R. Ponce Ortiz, M. R. Butler, P. L. Boudreault, J. Strzalka, P. O. Morin, M. Leclerc, J. T. Lopez Navarrete, M. A. Ratner, L. X. Chen, R. P. Chang, A. Facchetti and T. J. Marks, *J. Am. Chem. Soc.*, 2012, 134, 18427–18439.
39 S. Y. Son, Y. Kim, J. Lee, G.-Y. Lee, W.-T. Park, Y.-Y. Noh, C. E. Park and T. Park, *J. Am. Chem. Soc.*, 2016, 138, 8096–8103.
40 I. Osaka, M. Shimawaki, H. Mori, I. Doi, E. Miyazaki, T. Koganezawa and K. Takimiya, *J. Am. Chem. Soc.*, 2012, 134, 3498–3507.
41 Z. Ma, W. Sun, S. Himmelberger, K. Vandewal, Z. Tang, J. Bergqvist, A. Salleo, J. W. Andreasen, O. Inganäs, M. R. Andersson, C. Müller, F. Zhang and E. Wang, *Energy Environ. Sci.*, 2014, 7, 361–369.
42 H. Zhou, L. Yang, A. C. Stuart, S. C. Price, S. Liu and W. You, *Angew. Chem., Int. Ed.*, 2011, 50, 2995–2998.
43 D. Lee, S. W. Stone and J. P. Ferraris, *Chem. Commun.*, 2011, 47, 10987–10989.
44 Y. Zhou, K. Tvingstedt, F. Zhang, C. Du, W.-X. Ni, M. R. Andersson and O. Inganäs, *Adv. Funct. Mater.*, 2009, 19, 3293–3299.
45 Q. Fan, Y. Wang, M. Zhang, B. Wu, X. Guo, Y. Jiang, W. Li, B. Guo, C. Ye, W. Su, J. Fang, X. Ou, F. Liu, Z. Wei, T. C. Sum, T. P. Russell and Y. Li, *Adv. Mater.*, 2018, 30, 1704546.
46 B. Qi and J. Wang, *Phys. Chem. Chem. Phys.*, 2013, 15, 8972–8982.
47 J. D. Servaites, S. Yeganeh, T. J. Marks and M. A. Ratner, *Adv. Funct. Mater.*, 2010, 20, 97–104.
48 K. Vandewal, K. Tvingstedt, A. Gadisa, O. Inganäs and J. V. Manca, *Nat. Mater.*, 2009, 8, 904.
49 A. K. K. Kyaw, D. H. Wang, V. Gupta, W. L. Leong, L. Ke, G. C. Bazan and A. J. Heeger, *ACS Nano*, 2013, 7, 4569–4577.
50 P. W. M. Blom, V. D. Mihailetchi, L. J. A. Koster and D. E. Markov, *Adv. Mater.*, 2007, 19, 1551–1566.
51 C. M. Proctor, M. Kuik and T.-Q. Nguyen, *Prog. Polym. Sci.*, 2013, 38, 1941–1960.
52 A. K. Kyaw, D. H. Wang, D. Wynands, J. Zhang, T. Q. Nguyen, G. C. Bazan and A. J. Heeger, *Nano Lett.*, 2013, 13, 3796–3801.
53 L. Gao, Z.-G. Zhang, H. Bin, L. Xue, Y. Yang, C. Wang, F. Liu, T. P. Russell and Y. Li, *Adv. Mater.*, 2016, 28, 8288–8295.
54 H. Li, Y. Zhao, J. Fang, X. Zhu, B. Xia, K. Lu, Z. Wang, J. Zhang, X. Guo and Z. Wei, *Adv. Energy Mater.*, 2018, 8, 1702377.
55 Y. Kim, H. Hwang, N. K. Kim, K. Hwang, J. J. Park, G. I. Shin and D. Y. Kim, *Adv. Mater.*, 2018, 30, 1706557.